

Signature of Collective Plasma Effects in Beam-Driven QED Cascades

Kenan Qu,¹ Sebastian Meuren,^{1,2} and Nathaniel J. Fisch¹

¹*Department of Astrophysical Sciences, Princeton University, Princeton, New Jersey 08544, USA*

²*Stanford PULSE Institute, SLAC National Accelerator Laboratory, Menlo Park, CA 94025*

(Dated: December 21, 2024)

QED cascades play an important role in extreme astrophysical environments like magnetars. They can also be produced by passing a relativistic electron beam through an intense laser field. Signatures of collective pair plasma effects in these QED cascades are shown to appear in exquisite detail through plasma-induced frequency upshifts in the laser spectrum. Remarkably, these signatures can be detected even in small plasma volumes moving at relativistic speeds. Strong-field quantum and collective pair plasma effects can thus be explored with existing technology, provided that ultra-dense electron beams were co-located with multi-PW lasers.

PACS numbers: 36.40.Gk, 52.27.Ep, 52.40.Db

Introduction.— Intriguing astrophysical environments like magnetars [1, 2], binary neutron-star mergers [3, 4], and core-collapse supernovae explosions [5, 6] exhibit magnetic fields substantially exceeding the QED critical field $B_s = m^2 c^2 / (\hbar e) \approx 4.4 \times 10^9$ T, also known as the Schwinger field [7]. The recent discovery [8–13] that magnetars are indeed progenitors of Fast Radio Bursts (FRBs) [14–17] solves an enigmatic mystery [18, 19]. Understanding the plasma physics of these extreme environments [20–22], including for the emerging field of multi-messenger astronomy [23–27], is critical. In magnetars, strong-field QED cascades fill the magnetosphere with a relativistic electron-positron pair plasma [28–30]. However, the interplay between strong-field quantum and collective plasma effects in what might be called the *QED plasma regime* remains poorly understood [31].

There is thus strong motivation to elucidate the physics of magnetar-type QED cascades in laboratory experiments. These cascades can be produced by passing a relativistic electron beam through an intense laser field. In order to observe a magnetar-type QED cascade with exponentially growing electron, positron, and photon densities, the critical field has to be significantly exceeded [32]. However, multi-GeV electron beams can boost the field by a large Lorentz factor to expose the physics of the QED plasma regime even with laser intensities as low as 10^{22} Wcm $^{-2}$. When the QED critical field is reached in the particle rest frame, quantum corrections to synchrotron emission and pair production then become important [33–44].

Collective plasma effects play a large role when the plasma density becomes comparable to the critical one. We show that, in fact, the combination of a 3 PW laser and a 30 GeV electron beam produces a fast-moving quasi-neutral pair-plasma with density over 10 times the original beam density. This requires initial electron beam densities of about 10^{20} cm $^{-3}$, which can be produced with state-of-the-art technology [45]. For nanocoulomb bunch charges, typical for LINAC beams, this implies a volume

of plasma on the order of μm^3 .

However, while the facility requirements are relatively modest, the plasma effects are notoriously hard to observe. The plasma is moving at relativistic speed with a width comparable or smaller than the skin depth. Conventional detection methods, e.g., by observing plasma instabilities like the two-stream instability [46], the Weibel instability [47], or stimulated Brillouin scattering (SBS) [48], cannot be used with such small plasma volumes. To explore the QED plasma regime with existing technology requires a new kind of diagnostic.

As we show here, plasma-induced frequency upshifts in the laser spectrum in the time-varying pair plasma, both as it forms and as it radiates, inform importantly and in exquisite detail on the interplay between strong-field quantum and collective plasma effects. The frequency upshift occurs when the index of refraction in plasma changes suddenly [49–55]. Here, the pair production changes the particle density which increases the plasma frequency. In addition, quantum synchrotron radiation reduces the electron and positron energy, and hence their masses, which also increases the plasma frequency. As we show numerically, detailed signatures of both of these effects appear in the output laser field spectrum, which are then measurable at intensities as low as 10^{22} Wcm $^{-2}$.

Thus, remarkably, despite the small plasma volume and despite the relativistic plasma motion, signatures of the QED plasma regime might be identified experimentally with state-of-the-art technology. What emerges is a compelling argument for colocating laser and beam facilities to explore QED cascades in general and QED plasma regimes in particular. This approach is complementary to the all-optical laser-laser collision approach, which requires intensities above 10^{24} Wcm $^{-2}$ [56–67], and thus the more ambitious undertaking of 100 PW-scale laser facilities [68–70].

Frequency upshift.—Oscillations of the produced pair plasma reduce the optical permittivity and thus cause a laser frequency upshift if changes in the electron/positron density n_p or in the effective particle mass γm_e occur

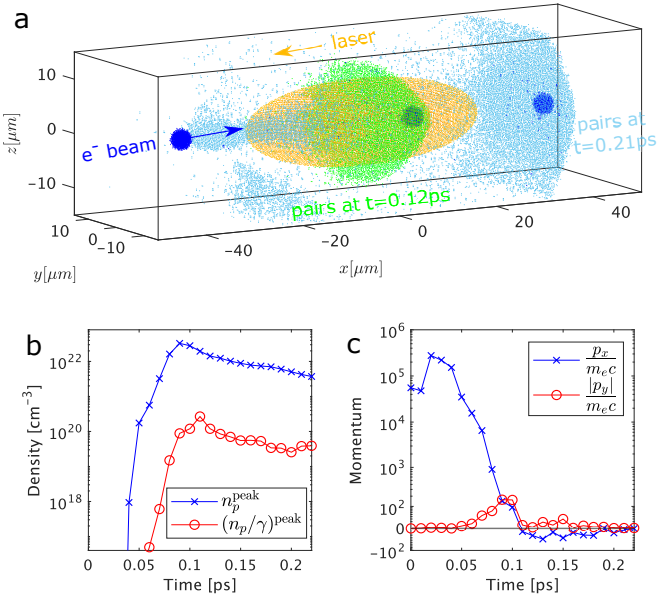


FIG. 1. **a** Schematics of the 3D QED-PIC simulation of a beam-driven cascade. An energetic electron beam (deep blue) collides with a multi-PW laser pulse (yellow) and creates an electron-positron pair plasma by inducing a QED cascade. The volume of the pair plasma at different times is denoted as green ($t = 0.12\text{ps}$) and light blue ($t = 0.21\text{ps}$) dots. **b** Evolution of the peak pair plasma density n_p (blue), and the parameter n_p/γ (red) which determines the laser frequency upshift. **c** Evolution of the pair particle momenta in the longitudinal (blue) and transverse (red) directions, normalized to $m_e c$.

non-adiabatically. Here m_e is the electron/positron rest mass and γ is the (instantaneous) Lorentz factor of the pair plasma. The relative frequency upshift is given by [71]

$$\Delta\tilde{\omega}^2 \equiv \omega_f^2/\omega_0^2 - 1 = 2n_p/(n_c\gamma), \quad (1)$$

where ω_0 (ω_f) is the initial (final) laser frequency, n_c is the critical plasma density for the input laser defined as $\omega_0^2 = e^2 n_c / (m_e \epsilon_0)$, $e > 0$ is the elementary charge, and ϵ_0 is the vacuum permittivity. Although frequency upconversion also causes a reduction of the laser intensity and a change of laser polarization [50, 55], experimental detection of these secondary effects is more challenging than measuring a shift of laser frequency.

Whereas an experimental measurement of the laser frequency shift can be made precisely, resolving the same small modification of the laser spectrum is very challenging with numerical particle-in-cell (PIC) simulations performed in discretized three-dimensional space. Here, we firstly focus on parameters which result in a clear numerical demonstration that the interplay between collective plasma and strong-field quantum effects leaves a characteristic imprint on the driving laser pulse. By verifying analytical scaling laws, we later substantiate that frequency upshift is already observable

at existing facilities with comparatively minor upgrades.

Initially, we consider a 1 nC electron beam of 300 GeV [72, 73], shown as a blue sphere in Fig. 1(a), which collides with a counter-propagating 24 PW laser pulse [69], shown as an amber spheroid (see methods section for more details). The electron beam sphere has an rms radius of 1 μm and a peak density of $n_e = 4 \times 10^{20} \text{ cm}^{-3}$ (Gaussian distribution). The Gaussian laser pulse is linearly polarized in the y direction and propagates in the $-x$ direction. The laser has a duration of 50 fs and a waist of 5 μm. The peak laser intensity is $6 \times 10^{22} \text{ W cm}^{-2}$, corresponding to a dimensionless amplitude $a_0 \equiv eE/(m_e c^2 \omega_0) \approx 170$. The simulations were performed with the QED module of the PIC code EPOCH [74] (see, e.g., [75] for general information on the QED-PIC methodology). As we show, these parameters will result in a nontrivial interplay between strong-field quantum and collective plasma phenomena, which causes very distinct measurable signatures.

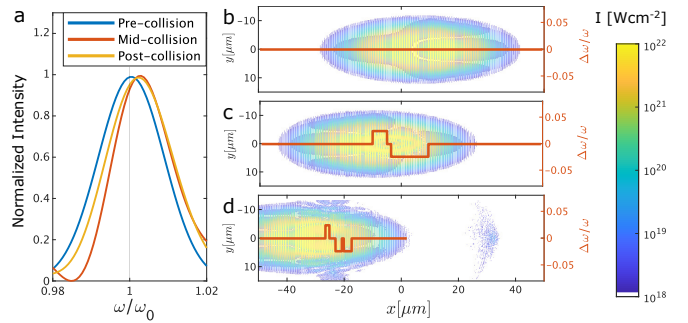


FIG. 2. **a** Normalized laser intensity spectra before, during, and after the laser pulse-electron beam collision. **b-d** Snapshots at $t = 0$ (**b**), $t = 0.12\text{ ps}$ (**c**), and $t = 0.21\text{ ps}$ (**d**). The pseudocolor plots show the laser beam profiles at the $z = 0$ cross section. The red curve shows the instantaneous laser frequency through a synchrosqueezed wavelet transform of the laser field at $y = z = 0$.

Pair generation and particle deceleration.—Inside the laser field, the electron beam is accelerated and therefore emits synchrotron radiation. In the classical regime ($\chi_e \ll 1$), electrons with energy \mathcal{E} typically emit photons with an energy $\hbar\omega \sim \chi_e \mathcal{E}$ [33, 76]. Here, the quantum parameter $\chi_e = E^*/E_s = \gamma|\mathbf{E}_\perp + \beta \times \mathbf{cB}|/E_s$ measures the electric field E^* in the electron rest frame in units of the critical field E_s [β is the electron velocity normalized to c , $\gamma = (1 - \beta^2)^{-1/2} = \mathcal{E}/(m_e c^2)$]. As soon as $\chi_e \gtrsim 0.1$ each emitted photon induces, on average, a substantial recoil, and quantum corrections become important. In the regime $\chi_e \gtrsim 1$, the quantum parameter of the emitted photon $\chi_\gamma = [\hbar\omega/(2m_e c^2)]|\mathbf{E}_\perp + \hat{\mathbf{k}} \times \mathbf{cB}|/E_s$ becomes, on average, comparable to unity and photon-induced pair production is sizable ($\hbar\mathbf{k}$ is the photon momentum) [33, 76].

When an electron beam collides with a laser pulse, a QED cascade is induced during the ramp-up of laser

intensity when $\chi_e \gtrsim 1$. It evolves into a pair plasma and its density continues to grow until the laser intensity ramps down. With an electron beam with energy $\mathcal{E}_0 = \gamma_0 m_e c^2$, the maximum quantum parameter scales linearly with the beam energy, *i.e.*, $\tilde{\chi}_e \approx 2a_0\gamma_0(\hbar\omega_0)/(m_e c^2)$. Although finite laser pulse waist and duration and finite pair creation time make it complicated to offer a simple relation of the final pair density, the linear scaling law $n_p \sim \tilde{\chi}_e n_e$ is reliable.

The parameters we use in Fig. 1 correspond to a quantum nonlinear parameter of $\tilde{\chi}_e \approx 220$ at the Gaussian waist in the focal plane, and $\tilde{\chi}_e \approx 600$ at the laser focus. The collision quickly creates a pair plasma with an increasing density and volume, illustrated at three different stages in Fig. 1a. To be precise, the peak plasma density, shown as blue curve in Fig. 1b, quickly grows to a peak value of $n_p = 82n_0 = 3.28 \times 10^{22} \text{ cm}^{-3}$ at $t = 0.09 \text{ ps}$. The total charge reaches a peak value of 139 nC. The plasma density then decreases due to plasma volume expansion. Due to this expansion, some of the particles no longer interact with the high intensity laser, which results in a lower total charge than $\tilde{\chi}_e n_e$.

However, the parameter n_p/γ , which determines the frequency upshift according to Eq. (1), continues to increase despite the decrease of n_p . It reaches the peak value of $2.67 \times 10^{20} \text{ cm}^{-3}$ at $t = 0.11 \text{ ps}$. Thus, the beneficial radiation friction force, which keeps reducing the gamma factor, outweighs the density increase between $t = 0.9 \text{ ps}$ and $t = 0.11 \text{ ps}$ until finally the latter effect dominates.

As photons with $\chi_\gamma \lesssim 1$ do not produce pairs, they will no longer contribute to the cascade. Electrons and positrons, however, will continue to lose energy via synchrotron radiation until $\chi_e \lesssim 0.1$. With a sufficiently long laser pulse, the pair gamma factor decreases asymptotically to

$$\gamma \lesssim 0.1 \frac{\gamma_0}{\tilde{\chi}_e} \approx \frac{0.05}{a_0} \frac{m_e c^2}{\hbar\omega_0}. \quad (2)$$

The effect of radiation friction is shown in Fig. 1c, where the blue curve shows that the pair particles rapidly lose longitudinal momentum before $t = 0.1 \text{ ps}$. At the same time, the pairs gain transverse momentum driven by the laser field, as indicated by the red curve. Notably, when the longitudinal and transverse momenta become comparable at $t = 0.11 \text{ ps}$, the pairs reverse direction.

Particle reflection.—The particle reflection is caused by the relativistic light pressure in the direction of the laser propagation direction. In a strong laser field, the transferable momentum from the laser photons to the particles scales as $m_e c [a_0^2/(4\gamma)]$ in a counter-propagating setup [33]. Therefore, the laser can stop and even reflect an electron if its gamma factor is reduced to $\gamma \sim a_0$ [77]. By comparing this condition with Eq. (2), we find that

particle reflection is possible if

$$a_0 \gtrsim \sqrt{0.05 m_e c^2 / (\hbar\omega_0)}. \quad (3)$$

For optical lasers with $\hbar\omega_0 \sim 1 \text{ eV}$, the threshold is approximately $a_0 \gtrsim 100$, corresponding to $I \gtrsim 10^{22}\text{-}10^{23} \text{ W cm}^{-2}$. Reflection of the plasma can be observed in Fig. 1c: the longitudinal momentum becomes negative at $t = 0.11 \text{ ps}$. This causes spreading of the pairs (shown as light blue dots) throughout the simulation box at $t = 0.21 \text{ ps}$.

At the point of particle reflection, the particle momentum is dominantly transverse, which arises from the laser acceleration. Hence, the minimum particle gamma factor is $\gamma \lesssim a_0$, although the exact value depends on the laser amplitude when the particles are reflected. Thus, we provide the following “rule of thumb” for the maximum achievable pair plasma density and the relevant gamma factor

$$n_p \sim \tilde{\chi}_e n_e, \quad \gamma_f \sim a_0. \quad (4)$$

These relations are valid if the laser is above the threshold intensity for particle reflection [Eq. (3)], and if the interaction time is long enough such that the cascade reaches its asymptotic state.

When the plasma density n_p or the Lorentz factor γ change non-adiabatically, the laser dispersion relation is modified and the laser frequency shifts correspondingly. As a result, the laser frequency increases in regions where the value (n_p/γ) increases. For the simulation under consideration, the peak value of n_p/γ corresponds to 6.7% of the critical plasma density at rest $n_c \approx 1.71 \times 10^{21} \text{ cm}^{-3}$ of the drive laser.

Accordingly, a laser frequency upshift is observed in the intensity spectra displayed in Fig. 2a. Comparing the spectra before and after the collision, their peaks show a shift of $\Delta\omega/\omega_0 = 0.2\%$. This finite frequency upshift is caused by the small fraction of laser overlap with the electron beam. Specifically, the frequency-upconverted photons are confined to a small region, whereas the majority of laser photons are not upconverted. To illustrate the laser photon frequencies at different pulse positions, we conduct a synchrosqueezed wavelet transform of the laser pulse and show the chirped spectra in Fig. 2b-d (red curves). Such a laser spectrogram is typically obtained in experiments using techniques like FROG [78] or SPIDER [79]. It can be seen that the flat topped input frequency spectrum (shown in Fig. 2b) becomes chirped at the region of plasma creation near $x = 0$ in Fig. 2c. The chirped region propagates along the laser direction. The maximum photon frequency shift reaches $\Delta\omega/\omega_0 = 2.4\%$.

Laser diffraction and back-scattering.—Noteworthy features shown in Fig. 2d are the side-scattering near $x = -25 \mu\text{m}$ and backward scattering near $x = 30 \mu\text{m}$. They are the combined result of the transverse acceleration

of the plasma by the laser and diffraction due to the small plasma size. The pair particles hence oscillate in the transverse direction and radiate in both the forward and backward directions. Since the pair plasma size is comparable to the laser wavelength, it causes strong diffraction as if the laser beam passes through a small aperture. Note that the largest impact results from the smallest particle energies when the plasma is stopped and eventually reflected.

Scaling laws.—Since upconversion of the laser frequency is determined by the pair creation/radiation friction and collective effects of the created pair plasma, it provides an unambiguous signature of collective plasma effects in beam-driven QED cascades. By combining the expression for the frequency upshift [Eq. (1)] with the scaling of the plasma parameters [Eq. (4)], we find

$$\Delta\omega^2 \sim \frac{2\tilde{\chi}_e n_e}{n_c a_0} \sim 4\gamma_0 \frac{\hbar\omega_0}{m_e c^2} \frac{n_e}{n_c} \quad (5)$$

for the frequency upshift. This relation holds if the laser pulse is sufficiently long and intense such that the QED cascade fully develops and the pair plasma is eventually stopped and reflected.

To verify Eq. (5), a series of 1D QED-PIC simulations were conducted with different electron beam densities, beam energies, and laser intensities. The results are shown in Fig. 3. In 1D simulations, transverse effects such as plasma inhomogeneity and laser diffraction are absent. But the particle momenta and currents are simulated in three dimensions, which is critical for inducing the laser frequency upshift.

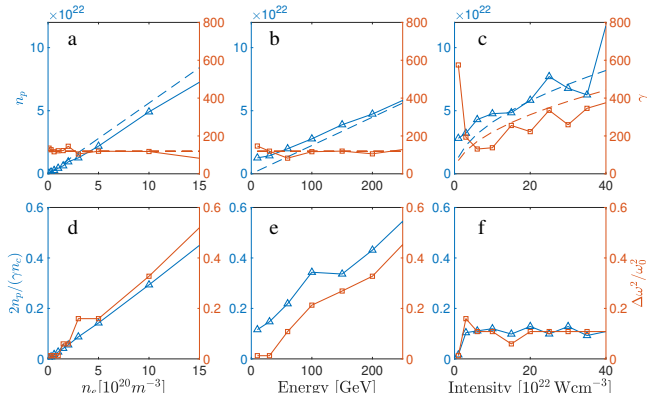


FIG. 3. The top row shows the dependence of the peak density n_p and Lorentz factor γ of the created pairs. The bottom row shows prediction and actual peak values of the relative frequency upshift of the laser pulses. The marked curves show the results obtained through 1D PIC simulations with the following parameters: electron beam peak density $n_p = 4 \times 10^{19} \text{ m}^{-3}$ (except in **a** and **d**), rms duration $1 \mu\text{m}/c$, energy 100 GeV (except in **b** and **e**); and laser peak intensity $3 \times 10^{22} \text{ Wcm}^{-2}$ (except in **d** and **f**), and duration 100 fs . The dashed curves show the theoretical values from Eqs. (4) and (1).

The simulation results shown Fig. 3a and 3b consider electron beams with varying peak densities and energies colliding with a laser pulse with peak amplitude $a_0 = 120$ ($3 \times 10^{22} \text{ Wcm}^{-2}$), respectively. As $\tilde{\chi}_e \propto \gamma_0$, either increasing beam density or beam energy causes a linear increase of the created pair plasma density, whereas the final gamma factor should remain constant at about a_0 . The results are in agreement with Eq. (4). The maximum frequency upshift shown in Fig. 3d, and 3e obtained from the synchrosqueezed wavelet transform also shows decent agreement with Eq. (5).

In Fig. 3c and 3f, the laser intensity I is varied from 10^{22} Wcm^{-2} ($a_0 = 70$) to $4 \times 10^{23} \text{ Wcm}^{-2}$ ($a_0 = 430$). For fixed electron beam energy the quantum parameter changes as $\tilde{\chi}_e \propto \sqrt{I}$. Therefore, we expect the final plasma density n_p to show a similar scaling. However, the quantity n_p/γ should be independent of the laser intensity if I is above the particle reflection threshold [Eq. (3)], as demonstrated in Fig. 3f. When the laser intensity is below $3 \times 10^{22} \text{ Wcm}^{-2}$, the pair reflection condition [Eq. (3)] is not satisfied and the cascade does not saturate within the pulse duration, causing a deviation from this scaling.

According to the “rule of thumb” [Eq. (5)], upshift of the instantaneous laser frequency becomes experimentally observable when the laser intensity is above $\sim 10^{22} \text{ Wcm}^{-2}$ and the electron beam density is above $\sim 10^{20} \text{ cm}^{-3}$. Such parameters require only a moderate upgrade of existing facilities, e.g., SLAC’s FACET-II [45]. Indeed, a separate set of 3D QED-PIC simulations show the prospect: 50 fs -duration, $2.5 \mu\text{m}$ -waist, a 3 PW ($3 \times 10^{22} \text{ Wcm}^{-2}$) laser pulse colliding with a 1nC , 30 GeV , $4 \times 10^{20} \text{ cm}^{-3}$ electron beam creates an electron-positron pair plasma of 19nC and peak density of $5 \times 10^{21} \text{ cm}^{-3}$. The parameter $2n_p/\gamma$ reaches $2 \times 10^{19} \text{ cm}^{-3}$, corresponding to 1.2% of the critical density of a $0.8 \mu\text{m}$ laser. Taking plasma expansion into account, the plasma oscillations of the *in situ* pair production could induce at least a 0.1% upshift of the instantaneous laser frequency. Our 3D-PIC simulations were not able to resolve this frequency shift directly due to limitations of computing resources. However, this upconversion can be inferred from our simulations and the scaling laws, and an experimental measurement would be straightforward.

In the electron-beam-laser collision setup, the produced pair plasma gets slowed down and, when the laser pulse is sufficiently strong and long, even reverses direction. The plasma reflection happens inhomogeneously, which creates counter-propagating plasma streams. The high density plasmas stream at low velocity thus exhibit a plethora of collective plasma effects. For example, we observe plasma filamentation arising from the Weibel instability [47] in the 3D QED-PIC simulations. When the plasma density parameter n_p/γ exceeds the critical density, the

plasma begins to reflect the driving laser similar to reflection by a relativistic electron mirror [80]. However, while fascinating, these phenomena are more difficult to measure quantitatively than frequency upshift of the driving laser itself. Nevertheless, the beam-laser collision setup, together with the proposed observable, opens seminal possibilities for studying laboratory astrophysics and High Energy Density Physics (HEDP) by providing access to the QED plasma regime with available technology.

This work was supported by NNSA Grant No. DE-NA0003871, and AFOSR Grant No. FA9550-15-1-0391. At Princeton, SM received funding from the Deutsche Forschungsgemeinschaft (DFG, German Research Foundation) under Grant No. 361969338. At Stanford, SM was supported by the U.S. Department of Energy under contract number DE-AC02-76SF00515.

-
- [1] V. M. Kaspi and A. M. Beloborodov, *Annu. Rev. Astron. Astrophys.* **55**, 261 (2017).
- [2] B. Cerutti and A. M. Beloborodov, *Space Sci. Rev.* **207**, 111 (2017).
- [3] Y. Q. Xue *et al.*, *Nature* **568**, 198 (2019).
- [4] D. J. Price and S. Rosswog, *Science* **312**, 719 (2006).
- [5] P. Mösta, C. D. Ott, D. Radice, L. F. Roberts, E. Schnetter, and R. Haas, *Nature* **528**, 376 (2015).
- [6] S. Akiyama, J. C. Wheeler, D. L. Meier, and I. Lichtenstadt, *Astrophys. J.* **584**, 954 (2003).
- [7] J. Schwinger, *Phys. Rev.* **82**, 664 (1951).
- [8] M. Tavani *et al.*, (2020), arXiv:2005.12164.
- [9] L. Lin *et al.*, (2020), arXiv:2005.11479.
- [10] A. Ridnaia *et al.*, (2020), arXiv:2005.11178.
- [11] C. K. Li *et al.*, (2020), arXiv:2005.11071.
- [12] C. D. Bochenek *et al.*, (2020), arXiv:2005.10828.
- [13] The CHIME/FRB Collaboration, (2020), arXiv:2005.10324.
- [14] B. Marcote *et al.*, *Nature* **577**, 190 (2020).
- [15] The CHIME/FRB Collaboration, *Nature* **566**, 235 (2019).
- [16] V. Ravi, M. Catha, L. D'Addario, S. G. Djorgovski, G. Hallinan, R. Hobbs, J. Kocz, S. R. Kulkarni, J. Shi, H. K. Vedantham, S. Weinreb, and D. P. Woody, *Nature* **572**, 352 (2019).
- [17] K. W. Bannister *et al.*, *Science* **365**, 565 (2019).
- [18] J. M. Cordes and S. Chatterjee, *Annu. Rev. Astron. Astrophys.* **57**, 417 (2019).
- [19] E. Petroff, J. W. T. Hessels, and D. R. Lorimer, *Astron. Astrophys. Rev.* **27**, 4 (2019).
- [20] D. A. Uzdensky and S. Rightley, *Rep. Prog. Phys.* **77**, 036902 (2014).
- [21] D. Uzdensky, M. Begelman, A. Beloborodov, R. Blandford, S. Boldyrev, B. Cerutti, F. Fiuzza, D. Giannios, T. Grismayer, M. Kunz, N. Loureiro, M. Lyutikov, M. Medvedev, M. Petropoulou, A. Philippov, E. Quataert, A. Schekochihin, K. Schoeffler, L. Silva, L. Sironi, A. Spitkovsky, G. Werner, V. Zhdankin, J. Zrake, and E. Zweibel, (2019), arXiv:1903.05328.
- [22] P. Zhang, S. S. Bulanov, D. Seipt, A. V. Arefiev, and A. G. R. Thomas, *Phys. Plasmas* **27**, 050601 (2020).
- [23] M.-H. Wang, S.-K. Ai, Z.-X. Li, N. Xing, H. Gao, and B. Zhang, *Astrophys. J.* **891**, L39 (2020).
- [24] B. P. Abbott *et al.*, *Astrophys. J.* **892**, L3 (2020).
- [25] LIGO Scientific Collaboration and Virgo Collaboration, *Phys. Rev. Lett.* **119**, 161101 (2017).
- [26] C. Palenzuela, L. Lehner, M. Ponce, S. L. Liebling, M. Anderson, D. Neilsen, and P. Motl, *Phys. Rev. Lett.* **111**, 061105 (2013).
- [27] M. Anderson, E. W. Hirschmann, L. Lehner, S. L. Liebling, P. M. Motl, D. Neilsen, C. Palenzuela, and J. E. Tohline, *Phys. Rev. Lett.* **100**, 191101 (2008).
- [28] A. Y. Chen, F. Cruz, and A. Spitkovsky, *Astrophys. J.* **889**, 69 (2020).
- [29] A. N. Timokhin and A. K. Harding, *Astrophys. J.* **871**, 12 (2019).
- [30] R. Guerout, Y. Shi, J.-M. Rax, and N. J. Fisch, *Nat. Commun.* **10**, 1 (2019).
- [31] D. B. Melrose and R. Yuen, *J. Plasma Phys.* **82**, 635820202 (2016).
- [32] V. Yakimenko, S. Meuren, F. Del Gaudio, C. Baumann, A. Fedotov, F. Fiuzza, T. Grismayer, M. J. Hogan, A. Pukhov, L. O. Silva, and G. White, *Phys. Rev. Lett.* **122**, 190404 (2019).
- [33] A. Di Piazza, C. Müller, K. Z. Hatsagortsyan, and C. H. Keitel, *Rev. Mod. Phys.* **84**, 1177 (2012).
- [34] I. V. Sokolov, N. M. Naumova, J. A. Nees, and G. A. Mourou, *Phys. Rev. Lett.* **105**, 195005 (2010).
- [35] H. Hu, C. Müller, and C. H. Keitel, *Phys. Rev. Lett.* **105**, 080401 (2010).
- [36] A. G. R. Thomas, C. P. Ridgers, S. S. Bulanov, B. J. Griffin, and S. P. D. Mangles, *Phys. Rev. X* **2**, 041004 (2012).
- [37] N. Neitz and A. Di Piazza, *Phys. Rev. Lett.* **111**, 054802 (2013).
- [38] S. S. Bulanov, C. B. Schroeder, E. Esarey, and W. P. Leemans, *Phys. Rev. A* **87**, 062110 (2013).
- [39] T. G. Blackburn, C. P. Ridgers, J. G. Kirk, and A. R. Bell, *Phys. Rev. Lett.* **112**, 015001 (2014).
- [40] D. G. Green and C. N. Harvey, *Phys. Rev. Lett.* **112**, 164801 (2014).
- [41] M. Vranic, J. L. Martins, J. Vieira, R. A. Fonseca, and L. O. Silva, *Phys. Rev. Lett.* **113**, 134801 (2014).
- [42] T. G. Blackburn, A. Ilderton, C. D. Murphy, and M. Marklund, *Phys. Rev. A* **96**, 022128 (2017).
- [43] M. Vranic, O. Klimo, G. Korn, and S. Weber, *Sci. Rep.* **8**, 4702 (2018).
- [44] J. Magnusson, A. Gonoskov, M. Marklund, T. Z. Esirkepov, J. K. Koga, K. Kondo, M. Kando, S. V. Bulanov, G. Korn, and S. S. Bulanov, *Phys. Rev. Lett.* **122**, 254801 (2019).
- [45] V. Yakimenko, L. Alsberg, E. Bong, G. Bouchard, C. Clarke, C. Emma, S. Green, C. Hast, M. J. Hogan, J. Seabury, N. Lipkowitz, B. O'Shea, D. Storey, G. White, and G. Yocky, *Phys. Rev. Accel. Beams* **22**, 101301 (2019).
- [46] R. G. Greaves and C. M. Surko, *Phys. Rev. Lett.* **75**, 3846 (1995).
- [47] B. D. Fried, *Phys. Fluids* **2**, 337 (1959).
- [48] M. R. Edwards, N. J. Fisch, and J. M. Mikhailova, *Phys. Rev. Lett.* **116**, 015004 (2016).
- [49] S. C. Wilks, J. M. Dawson, and W. B. Mori, *Phys. Rev. Lett.* **61**, 337 (1988).

- [50] K. Qu and N. J. Fisch, *Phys. Plasmas* **26**, 083105 (2019).
- [51] M. R. Shcherbakov, K. Werner, Z. Fan, N. Talisa, E. Chowdhury, and G. Shvets, *Nat. Commun.* **10**, 1345 (2019).
- [52] A. Nishida, N. Yugami, T. Higashiguchi, T. Otsuka, F. Suzuki, M. Nakata, Y. Sentoku, and R. Kodama, *Appl. Phys. Lett.* **101**, 161118 (2012).
- [53] K. Qu, Q. Jia, M. R. Edwards, and N. J. Fisch, *Phys. Rev. E* **98**, 023202 (2018).
- [54] M. R. Edwards, K. Qu, Q. Jia, J. M. Mikhailova, and N. J. Fisch, *Phys. Plasmas* **25**, 053102 (2018).
- [55] S. S. Bulanov, A. M. Fedotov, and F. Pegoraro, *Phys. Rev. E* **71**, 016404 (2005).
- [56] A. R. Bell and J. G. Kirk, *Phys. Rev. Lett.* **101**, 200403 (2008).
- [57] A. M. Fedotov, N. B. Narozhny, G. Mourou, and G. Korn, *Phys. Rev. Lett.* **105**, 080402 (2010).
- [58] S. S. Bulanov, T. Z. Esirkepov, A. G. R. Thomas, J. K. Koga, and S. V. Bulanov, *Phys. Rev. Lett.* **105**, 220407 (2010).
- [59] E. N. Nerush, I. Y. Kostyukov, A. M. Fedotov, N. B. Narozhny, N. V. Elkina, and H. Ruhl, *Phys. Rev. Lett.* **106**, 035001 (2011).
- [60] N. V. Elkina, A. M. Fedotov, I. Y. Kostyukov, M. V. Legkov, N. B. Narozhny, E. N. Nerush, and H. Ruhl, *Phys. Rev. Spec. Top. Accel. Beams* **14**, 054401 (2011).
- [61] M. Jirka, O. Klimo, S. V. Bulanov, T. Z. Esirkepov, E. Gelfer, S. S. Bulanov, S. Weber, and G. Korn, *Phys. Rev. E* **93**, 023207 (2016).
- [62] T. Grismayer, M. Vranic, J. L. Martins, R. A. Fonseca, and L. O. Silva, *Phys. Plasmas* **23**, 056706 (2016).
- [63] X.-L. Zhu, T.-P. Yu, Z.-M. Sheng, Y. Yin, I. C. E. Turcu, and A. Pukhov, *Nat. Commun.* **7**, 1 (2016).
- [64] M. Tamburini, A. D. Piazza, and C. H. Keitel, *Sci. Rep.* **7**, 1 (2017).
- [65] A. Gonoskov, A. Bashinov, S. Bastrakov, E. Efimenko, A. Ilderton, A. Kim, M. Marklund, I. Meyerov, A. Muraviev, and A. Sergeev, *Phys. Rev. X* **7**, 041003 (2017).
- [66] T. Grismayer, M. Vranic, J. L. Martins, R. A. Fonseca, and L. O. Silva, *Phys. Rev. E* **95**, 023210 (2017).
- [67] A. F. Savin, A. J. Ross, R. Aboushelbaya, M. W. Mayr, B. Spiers, R. H.-W. Wang, and P. A. Norreys, *Sci. Rep.* **9**, 1 (2019).
- [68] E. Cartlidge, *Science* **359**, 382 (2018).
- [69] J. Bromage, S.-W. Bahk, I. A. Begishev, C. Dorner, M. J. Guardalben, B. N. Hoffman, J. Oliver, R. G. Roides, E. M. Schiesser, M. J. Shoup III, and et al., *High Power Laser Sci.* **7**, e4 (2019).
- [70] C. N. Danson, C. Haefner, J. Bromage, T. Butcher, J.-C. F. Chanteloup, E. A. Chowdhury, A. Galvanauskas, L. A. Gizzi, J. Hein, D. I. Hillier, N. W. Hopps, Y. Kato, E. A. Khazanov, R. Kodama, G. Korn, R. Li, Y. Li, J. Limpert, J. Ma, C. H. Nam, D. Neely, D. Papadopoulos, R. R. Penman, L. Qian, J. J. Rocca, A. A. Shaykin, C. W. Siders, C. Spindloe, S. Szatmári, R. M. G. M. Trines, J. Zhu, P. Zhu, and J. D. Zuegel, *High Power Laser Sci. Eng.* **7**, e54 (2019).
- [71] W. L. Kruer, *The physics of laser plasma interactions* (Westview Press, 2003).
- [72] M. Aicheler, P. Burrows, M. Draper, T. Garvey, P. Lebrun, K. Peach, N. Phinney, H. Schmidkler, D. Schulte, and N. Toge, *A Multi-TeV Linear Collider Based on CLIC Technology: CLIC Conceptual Design Report*, CERN Yellow Reports: Monographs (CERN, Geneva, 2012).
- [73] A. Caldwell, K. Lotov, A. Pukhov, and F. Simon, *Nature Phys.* **5**, 363 (2009).
- [74] T. D. Arber, K. Bennett, C. S. Brady, A. Lawrence-Douglas, M. G. Ramsay, N. J. Sircombe, P. Gillies, R. G. Evans, H. Schmitz, A. R. Bell, et al., *Plasma Phy. Contr. F.* **57**, 113001 (2015).
- [75] A. Gonoskov, S. Bastrakov, E. Efimenko, A. Ilderton, M. Marklund, I. Meyerov, A. Muraviev, A. Sergeev, I. Surmin, and E. Wallin, *Phys. Rev. E* **92**, 023305 (2015).
- [76] V. B. Berestetskii, E. M. Lifshitz, and L. P. Pitaevskii, *Quantum Electrodynamics*, 2nd ed. (Butterworth-Heinemann, 1982).
- [77] J.-X. Li, K. Z. Hatsagortsyan, B. J. Galow, and C. H. Keitel, *Phys. Rev. Lett.* **115**, 204801 (2015).
- [78] D. J. Kane and R. Trebino, *IEEE J. Quantum Electron* **29**, 571 (1993).
- [79] C. Iaconis and I. A. Walmsley, *Opt. Lett.* **23**, 792 (1998).
- [80] D. Kiefer, M. Yeung, T. Dzelzainis, P. S. Foster, S. G. Rykovanov, C. L. Lewis, R. S. Marjoribanks, H. Ruhl, D. Habs, J. Schreiber, M. Zepf, and B. Dromey, *Nat. Commun.* **4**, 1763 (2013).